AGU PUBLICATIONS

Geochemistry, Geophysics, Geosystems

RESEARCH ARTICLE
10.1002/2013GC005179

Key Points:
- Gas analyses show thermogenic methane emanates into the water column
- A shallow THSZ results in hydrate-rimmed bubble transport to shallow depths
- A rough BHSZ may result in enhanced sensitivity of hydrates to warming

Correspondence to:
A. J. Smith,
andrew.j.smith.6022@gmail.com

Citation:
Smith, A. J., J. Mienert, S. Bünz, and J. Greinert (2014), Thermogenic methane injection via bubble transport into the upper Arctic Ocean from the hydrate-charged Vestnesa Ridge, Svalbard, *Geochem. Geophys. Geosyst.*, *15*, 1945–1959, doi:10.1002/2013GC005179.

Received 3 DEC 2013
Accepted 16 APR 2014
Accepted article online 21 APR 2014
Published online 29 MAY 2014

Thermogenic methane injection via bubble transport into the upper Arctic Ocean from the hydrate-charged Vestnesa Ridge, Svalbard

Andrew J. Smith[1], Jürgen Mienert[1], Stefan Bünz[1], and Jens Greinert[1,2,3]

[1]Centre for Arctic Gas Hydrate, Environment and Climate, UiT The Arctic University of Norway, Tromsø, Norway, [2]Department of Marine Geology, Royal Netherlands Institute for Sea Research, Texel, Netherlands, [3]Department of Marine Geosystems, GEOMAR Helmholtz Centre for Ocean Research Kiel, Kiel, Germany

Abstract We use new gas-hydrate geochemistry analyses, echosounder data, and three-dimensional P-Cable seismic data to study a gas-hydrate and free-gas system in 1200 m water depth at the Vestnesa Ridge offshore NW Svalbard. Geochemical measurements of gas from hydrates collected at the ridge revealed a thermogenic source. The presence of thermogenic gas and temperatures of ~3.3°C result in a shallow top of the hydrate stability zone (THSZ) at ~340 m below sea level (mbsl). Therefore, hydrate-skinned gas bubbles, which inhibit gas-dissolution processes, are thermodynamically stable to this shallow water depth. This was confirmed by hydroacoustic observations of flares in 2010 and 2012 reaching water depths between 210 and 480 mbsl. At the seafloor, bubbles are released from acoustically transparent zones in the seismic data, which we interpret as regions where free gas is migrating through the hydrate stability zone (HSZ). These intrusions result in vertical variations in the base of the HSZ (BHSZ) of up to ~150 m, possibly making the shallow hydrate reservoir more susceptible to warming. Such Arctic gas-hydrate and free-gas systems are important because of their potential role in climate change and in fueling marine life, but remain largely understudied due to limited data coverage in seasonally ice-covered Arctic environments.

1. Introduction

Gas hydrate is an ice-like compound found in marine sediments where high pressures, low temperatures, ample supplies of water, and guest molecules such as CH_4, C_2H_6, C_3H_8, CO_2, and H_2S coexist [*Sloan*, 1998]. Hydrates may be a future energy resource [*Milkov and Sassen*, 2002], and hydrate dissociation may have caused past environmental change [*Dickens*, 2003; *Kennett et al*., 2000] and slope failure [*Kayen and Lee*, 1991]. Present-day ocean warming may be causing hydrate dissociation and massive methane release offshore the Eastern U.S. [*Phrampus and Hornbach*, 2012] and in the Arctic [*Ferré et al*., 2012; *Marín-Moreno et al*., 2013; *Shakhova et al*., 2013; *Westbrook et al*., 2009].

In recent years, Arctic hydrate deposits have received intense scientific attention because of warming in the Arctic that is occurring at a rate ~2× faster than at lower latitudes [e.g., *Graversen et al*., 2008]. Much of this focus has been directed toward hydrates at the landward termination of the HSZ because of their high sensitivity to ocean warming and proximity to the atmosphere in shallow water [e.g., *Berndt et al*., 2014; *Gentz et al*., 2014; *Mienert et al*., 2005; *Phrampus and Hornbach*, 2012; *Westbrook et al*., 2009]. Methane release from deepwater hydrates, however, has generally been neglected even though >95% of the Arctic's hydrate reservoir exists in the deepwater [*Ruppel*, 2011]. This is because of the long time (<1000 years) required for seafloor temperature changes to thermally equilibrate within the HSZ [*Reagan and Moridis*, 2007] and to the efficiency of the sediments and water column as a biologically mediated methane filter [*Kessler et al*., 2011; *Reeburgh*, 2007]. Deepwater Arctic hydrate deposits, however, remain understudied, and long-term monitoring of such systems is still needed to better understand their sensitivity to ocean warming and the extent to which they can deliver methane to the upper ocean.

Here we focus on the role of deepwater free-gas and gas-hydrate systems in the Arctic for delivering methane to the upper ocean. Since the first observations of rising hydrate and bubble plumes in the Guaymas Basin [*Lonsdale and Becker*, 1985; *Merewether et al*., 1985], bubble plumes have been observed rising from hydrate deposits around the world [*Berndt et al*., 2014; *Brothers et al*., 2013; *Greinert et al*., 2006, 2010; *Römer*

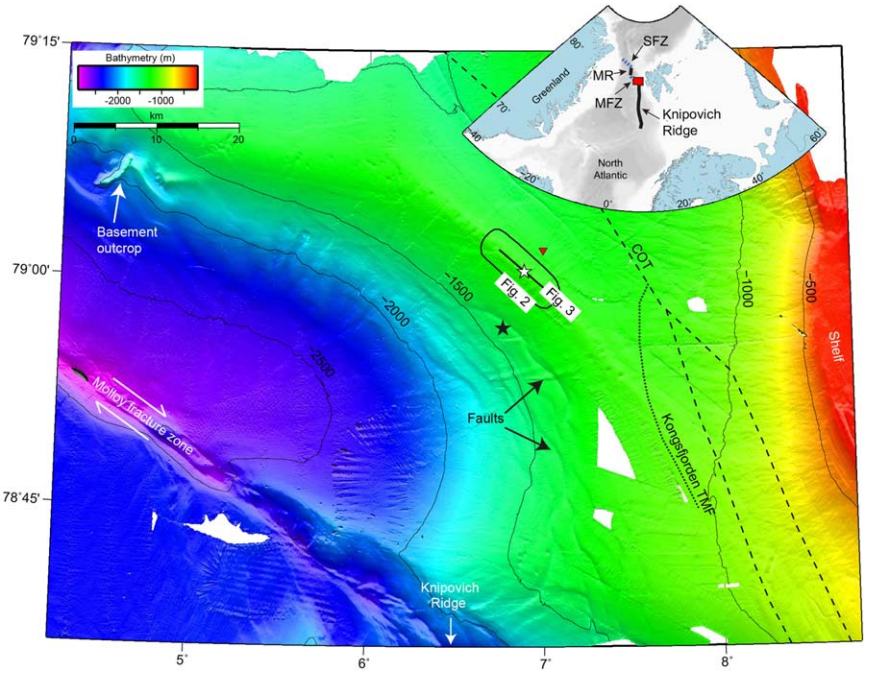

Figure 1. Bathymetric map of the Vestnesa Ridge, offshore NW-Svalbard. The Vestnesa Ridge is a sediment drift that lies on <20 Ma old oceanic crust [*Hustoft et al*., 2009], located to the northeast of the Molloy Fracture Zone (MFZ) and to the east of the slow-spreading Molloy Ridge (MR; inset). Upper inset also shows the location of the Spitsbergen Fracture Zone (SFZ) and the Knipovich Ridge. The propagation of the Knipovich Ridge to the north and/or thermal subsidence of the oceanic basin may be responsible for faulting of sedimentary cover (black arrows) [*Hustoft et al*., 2009]. The continent-to-ocean transition (COT) is shown with a dashed black line, and the seaward extent of the Kongsfjorden trough-mouth fan (TMF) is indicated with a dotted black line. Overlain on the map are locations of CTD measurements between 2010 (white star) and 2012 (black star) and a sediment temperature profile (102°C km^{-1}, inverted red triangle) [*Sundvor et al*., 2000].

et al., 2012; *Sauter et al*., 2006; *Westbrook et al*., 2009]. Within the HSZ, hydrate rims may develop around these bubbles, inhibit gas-dissolution processes and allow bubbles to reach heights as great as 1300 m above the seafloor [*Greinert et al*., 2006]. If bubble transport is further aided by an oily layer, bubbles may reach the ocean surface and export considerable amounts of methane directly to the atmosphere [*Solomon et al*., 2009]. We analyze one example of a free-gas and gas-hydrate system at the Vestnesa Ridge in 1200 m water depth, offshore NW Svalbard, where seafloor bubble release has been previously documented [*Bünz et al*., 2012; *Hustoft et al*., 2009]. We present new gas-hydrate geochemistry analyses, four-dimensional echosounder data (from 2010 to 2012), and previously published three-dimensional P-Cable seismic data [*Bünz et al*., 2012] to study the extent to which this deepwater Arctic location can deliver methane to the upper ocean and possibly atmosphere. We also evaluate the sensitivity of this deepwater hydrate system to a seafloor-warming scenario.

2. Study Area

The Vestnesa Ridge is a gas-hydrate system located on hot (115 mW m^{-2}) and young (<20 Ma) oceanic crust of the eastern spreading center of the Molloy Ridge [*Hustoft et al*., 2009; *Sundvor et al*., 2000]. The ridge is bounded by a continent-ocean transition to the northeast and by the active Molloy Fracture Zone and Knipovich Ridge to the south and southeast, respectively (Figure 1). The ridge extends 50–60 km from the northwest to the southeast and is comprised of a postrift sedimentary succession that is up to 5 km thick [*Eiken and Hinz*, 1993; *Hustoft et al*., 2009].

Deepwater hydrated sediments at the Vestnesa Ridge span an area of ~3000 km^2 and comprise a methane reservoir of 0.5–0.9 Gt [*Hustoft et al*., 2009]. A climate-sensitive shallow gas-hydrate system lies adjacent to Vestnesa and is in 350–800 m water depth and may release 5.3–29 $\times$ 10^{-6} Gt yr^{-1} of methane over the next three centuries [*Marín-Moreno et al*., 2013]. The deepwater ridge is spotted with pockmarks that are hundreds of

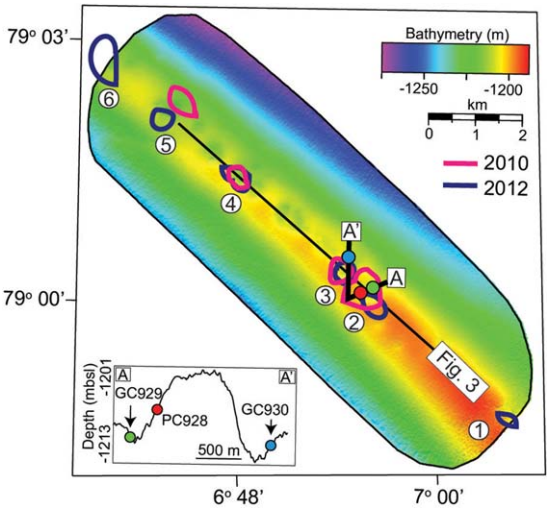

Figure 2. Bathymetric map with flare and coring locations. Map shows the location of flares that we observed in 2010 (bold pink lines) and 2012 (bold blue lines), gravity cores that retrieved hydrates (GC929) and Pogonphora (Siboglinidae) and Beggiatoa bacterial mats (GC930), and a piston core that retrieved methane-derived carbonate crusts (PC928). Numbers label active pockmarks. Lower inset shows bathymetric profile and coring locations within pockmarks.

meters in diameter and tens of meters in vertical relief [*Bünz et al.*, 2012; *Vogt et al.*, 1994] (Figure 2). A bottom-simulating reflector (BSR), interpreted to record a negative impedance contrast between gas hydrate above and free gas below, is present below the ridge [*Bünz et al.*, 2012; *Hustoft et al.*, 2009] (Figure 3b, modified after *Bünz et al.* [2012]). Gas bubbles were first reported to emanate from the seafloor in September 2008 [*Schiermeier*, 2008] and in October 2008 during the UiT R/V Helmer Hanssen cruise using the 18 kHz signal of the Simrad EK60 echosounder [*Hustoft et al.*, 2009], after surveys in 2006 and 2007 using the same EK60 echosounder failed to detect any bubble release [*Hustoft et al.*, 2009].

3. Methods

We acquired new hydroacoustic and CTD data as well as sediment samples aboard the R/V Helmer Hanssen, operated by UiT, during one research expedition in June 2010 and two expeditions in June/July 2012. The hydroacoustic information consists of bathymetric data and single-beam echosounder data. Bathymetry data displayed in Figure 1 were acquired on preceding R/V Helmer Hanssen cruises [*Hustoft et al.*, 2009].

3.1. Hydroacoustics

We acquired new swath bathymetry data (Figures 1, 2, 4, and 5) using the Kongsberg Simrad EM300 system. This system operates at a frequency of 30 kHz with an angular coverage of ~135°. Data were processed using Kongsberg Neptune software. Gridding (10 m for 2010 and 2012 data sets shown in Figures 2, 4, and 5; 50 m for regional data set shown in Figure 1) and imaging of the data were done using Generic Mapping Tools (GMT). Visualization was performed using QPS Fledermaus software.

Single-beam echosounder data were acquired using a Simrad EK60 system operating at frequencies of 18, 38, and 120 kHz. As a result of the high impedance contrast between water and free gas, this system can ideally be used to detect gas bubbles in the water column that are recorded as "acoustic flares" [*Greinert et al.*, 2006]. These flares can be produced from a single bubble stream or from multiple streams of rising bubbles. Raw data were stored with the ER60 software from Kongsberg and processed with QPS FMMidwater. Flare heights were measured in FMMidwater software, and the three-dimensional shape of flares was visualized in Fledermaus.

A persistent issue related to the hydroacoustic detection of gas-bubble plumes is whether we really measure the highest point that bubbles rise and dissolve. The used single-beam echosounder has a beam angle of ~6.5°, and yet rising bubbles are displaced horizontally due to currents. We can therefore not be sure that the top of flares presents the highest point to which bubbles rise and dissolve. Furthermore, the height of flares detected by the echosounder strongly depends on the frequency of the sound source [*Greinert et al.*, 2010]. We observe, however, very good agreement in both the maximum bubble rise height detected during SW-NE passes over the Vestnesa Ridge and SE-NW passes over the ridge. Because of these similar readings and also because of the rather symmetrical shape of the flares, we are confident that we detected the top of the flares. We measured the flare height with the 38 kHz echosounder signal. However, it is likely that some smaller bubbles reach heights that are higher than the detected flare top if bubbles are smaller than the resonance frequency [*Greinert et al.*, 2006, 2010] (here: ~0.8 and 1.2 mm diameter at 210 and 480 m water depth, respectively).

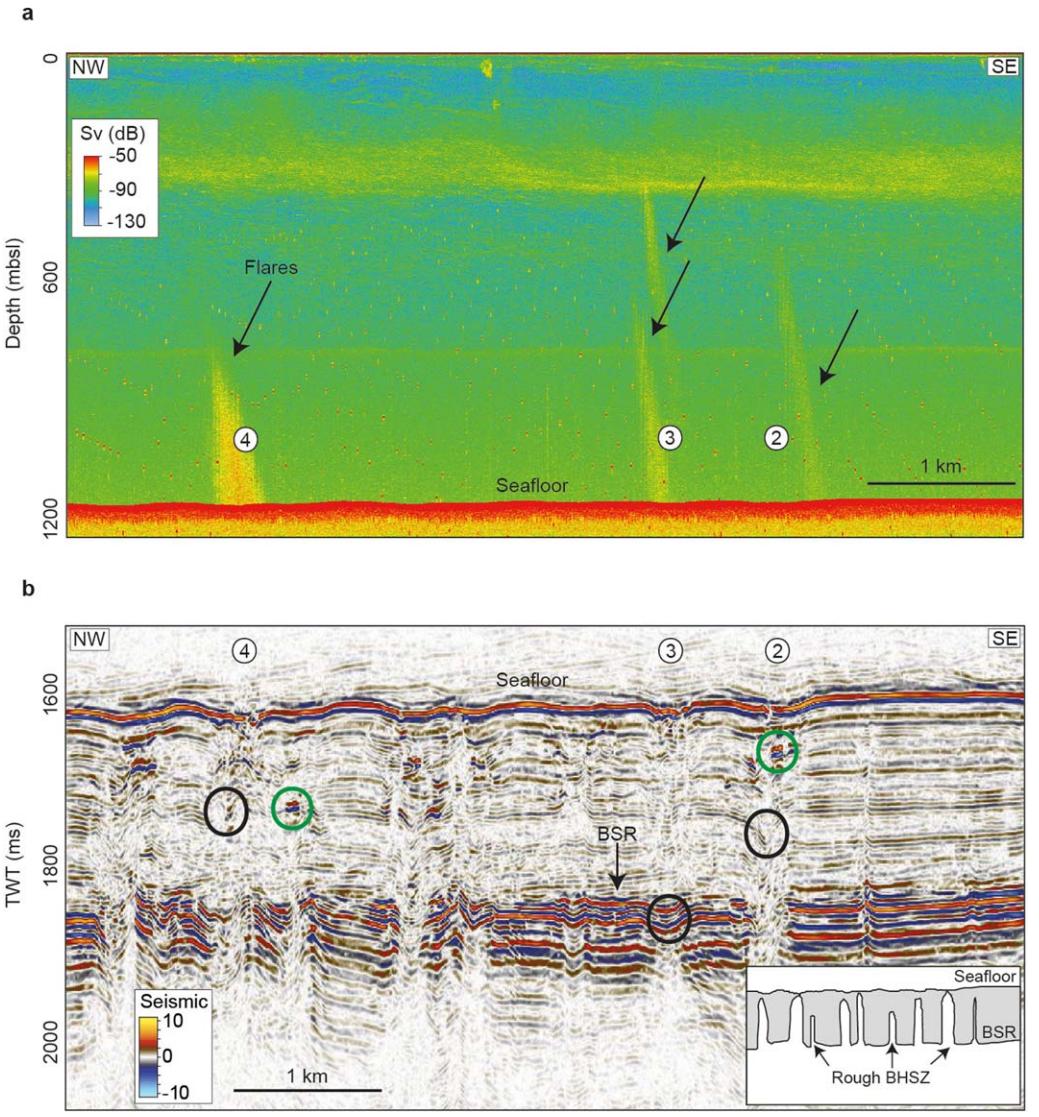

Figure 3. Acoustic anomalies in the water and sediment columns. (a) An echogram of the 2012 survey (38 kHz) at the Vestnesa Ridge shows examples of flares (black arrows). The volume backscattering strength of the received sound signal (Sv) is given by the color of the bubble plumes. The flares show a deflection toward the North due to the bottom-water current (8 cm s^{-1}) [*Fahrbach et al.*, 2001] in the eastern Fram Strait. (b) Example of a seismic reflection profile through pockmarks from a 2010 3-D P-Cable Survey [*Bünz et al.*, 2012] with two-way traveltime (TWT) on the vertical axis. Enhanced reflections (green circles) and "push-down" features (black circles) are present within the HSZ. We interpret these features to record the presence of free gas. Acoustically transparent zones, interpreted as gas chimneys, extend from the seafloor to depths below the BSR. These gas-rich vertical intrusions create significant lateral variations in the BHSZ (inset). The location of flares coincides with areas where chimneys are visible in the seismic data; however, there are several gas chimneys above which no flares are present. Location of echogram and reflection profile is shown in Figures 1 and 2.

3.2. CTD

To acquire physical water-column data, a SeaBird SBE 9 was deployed in 2010 on the Vestnesa Ridge and in 2012 adjacent to the ridge (Figure 1). The CTD measures temperature, salinity, and pressure continuously; the sound velocity was calculated from these measurements as input for bathymetric processing. Because our 2010 measurement is taken closer to the crest of the Vestnesa Ridge, we use temperature and salinity data from this CTD cast for modeling of the HSZ and the bubble-dissolution simulations.

3.3. Coring and Gas Geochemistry

In 2012, we performed piston coring (PC) and gravity coring (GC) of sediments in the upper few meters below seafloor in an attempt to recover gas hydrates, methane-derived carbonates, and/or methane-seepage-influenced benthic foraminifera. Upon recovery of gas hydrate, small gas-hydrate flakes were

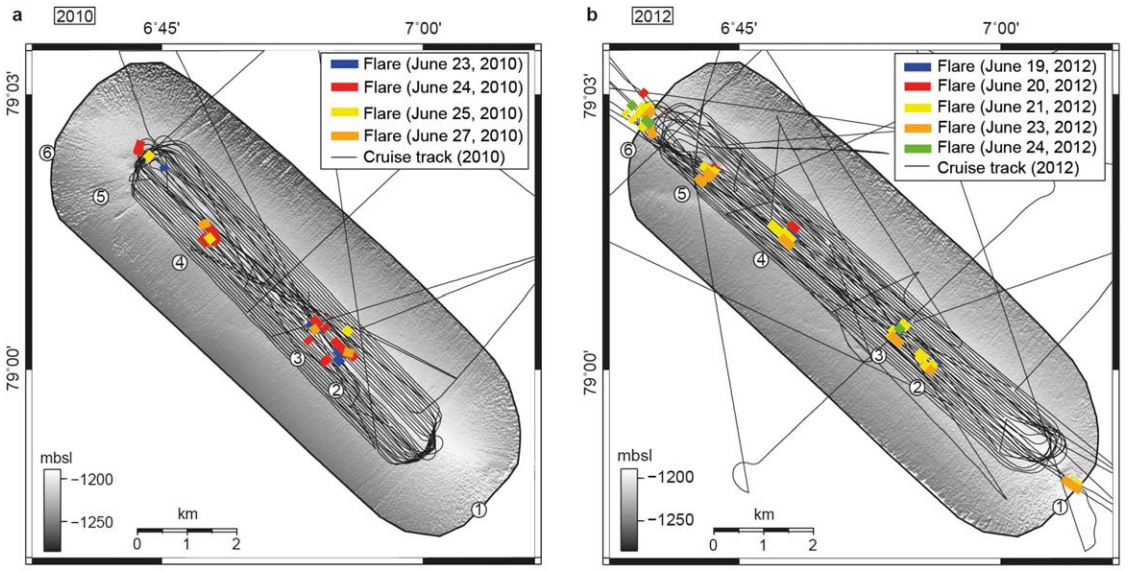

Figure 4. Cruise track and flare occurrences during (a) 2010 and (b) 2012. There were no noticeable, hourly or daily variations in bubble release from the pockmarks, indicating that seepage from the pockmarks does not undergo short-term variations. The activity of pockmarks 1 and 6 could not be proven for 2010 due to the smaller area covered with the survey during that cruise.

handpicked from the sediment immediately after opening the core and were transferred into 20 mL head space glass vials which held 3 mL of super saturated NaCl solution. The developing overpressure was released by slightly lifting the inserted rubber stopper. After complete dissociation of the hydrate, the vials were crimped gas tight and stored topside over until further analyses in onshore labs at Royal NIOZ and GEOMAR. Gas composition analyses were undertaken by gas chromatography with an FID detector using a ThermoScientific FOCUS GC (temperature ramping 40, 70, and 120°C; H_2 carrier gas, Resteck 2 m packed column HS-Q 80/100). Accuracy of the method and system is 5% for methane and 8% for ethane and propane.

Stable carbon isotope ratios of methane were determined by using a continuous flow GC-IRMS combination. Methane and ethane were separated in a Thermo Trace GC (Isotherm at 70°C, He-carrier gas, ShinCarbon 1.5 m packed column). The subsequent conversion of methane and ethane, respectively, to carbon dioxide was conducted in a Ni/Pt combustion furnace at 980°C. The δ^{13}C-value of produced CO_2 was

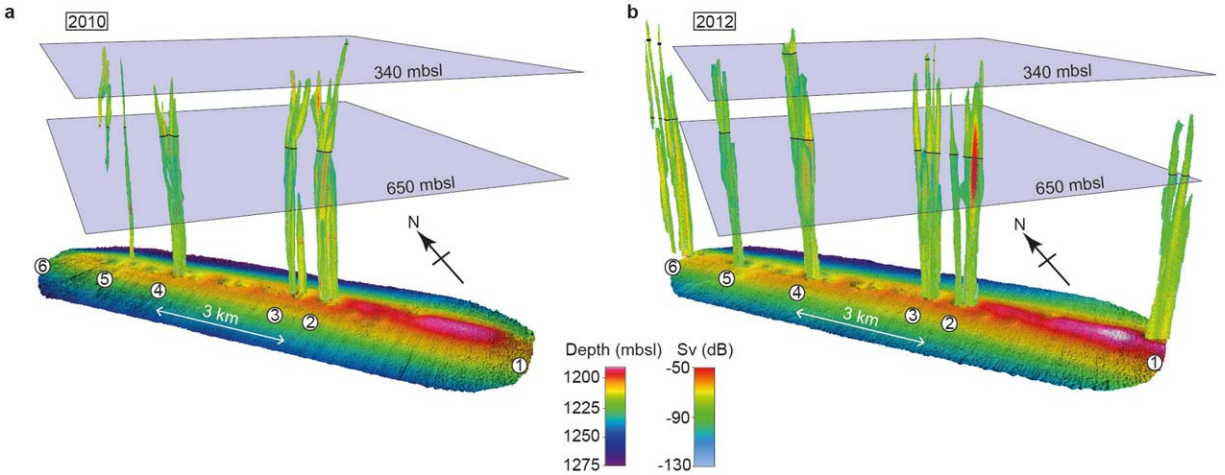

Figure 5. Flares above pockmarks at the Vestnesa Ridge in (a) 2010 and (b) 2012. Flares showed volume backscattering strengths (Sv) of up to −50 dB. Besides the slight offset in seafloor depths between 2010 and 2012, which is within the vertical error of the multibeam system (±3 m), there was no noticeable difference in seafloor morphology.

determined by isotope ratio mass spectrometry (Thermo MAT253). Reproducibility of stable carbon isotope determination is about $\pm 0.3‰$. All isotope ratios are given in the d-notation versus Vienna Pee Dee Belemnite (VPDB) standard. Isotope ratios and gas compositions are reported as averages from three samples, which agreed well with each other.

3.4. Constraining the Composition of the Thermogenic Feed Gas and the HSZ

Molecular fractionation occurs during gas-hydrate crystallization, resulting in a preferred incorporation of larger gas molecules into the water cages of the gas-hydrate structure [*Sloan*, 1998]. As a result, hydrates will be enriched in heavier hydrocarbons and depleted in C_1 compared to the original feed gas that is supplied from below the HSZ. We use the CSMYHD program [*Sloan*, 1998] to theoretically solve for this original feed-gas composition necessary to form hydrates with the measured molecular gas composition. The estimated original gas composition was used together with CTD measurements and previously measured seafloor temperature gradients from the study area [*Sundvor et al*., 2000] to constrain the depth of the top and base of the HSZ.

3.5. Single Bubble-Dissolution Model

The numerical bubble-dissolution model accounts for hydrate-skin effects on bubble transport within the HSZ and is described in detail by *McGinnis et al*. [2006]. The model predicts evolving bubble size, gas composition, and rise distance. It is suitable for nearly all aquatic environments and has been validated with direct observations in the saline deepwater [*McGinnis et al*., 2006]. For the model, we define salinity and temperature within the water column using a CTD cast from 2010 (Figure 1). The THSZ is constrained with gas-hydrate geochemistry data. We assume the bubble is initially comprised of 100% CH_4. CH_4 and O_2 concentrations were derived from headspace water sampling (ranging from 3 nM at the sea surface to 1.2 nM at the bottom) and a Seabird SBE43 O_2 sensor (ranging from 0.27 to 0.26 mol L^{-1}). Nitrogen was calculated to be saturated throughout the water column. These values are consistent with measured values in the deepwater offshore NW-Svalbard [*Damm et al*., 2005] and are approximately averages for other marine basins [*Greinert and McGinnis*, 2009; *McGinnis et al*., 2006]. The initial bubble size was adjusted until the model predicted bubble-rise heights similar to those observed in our echosounder data.

4. Results and Discussion

4.1. Gas Flares

During both the 2010 and 2012 cruises which each lasted 4–5 days, we discovered rising gas bubbles in the water column at 4 separate pockmarks in 2010 and at 6 pockmarks in 2012 (Figures 2, 3a, 4, and 5). In 2010, we detected a total of 21 flares emanating from 4 separate pockmarks (pockmarks 2–5; Figure 4). Gas release at pockmark 2 appeared to be the most active: seven flares were observed from just this pockmark, and seepage appeared to occur over the largest area (Figures 2 and 4). A total of 4, 5, and 5 flares were observed at pockmarks 3, 4, and 5, respectively (Figure 4). In 2012, we detected a total of 36 flares from the 6 pockmarks. Pockmark 6 was the most active with a total of 10 flares. We observed 3, 7, 6, 5, and 5 flares at pockmarks 1–5, respectively (Figure 4). It is unclear if pockmarks 1 and 6 were active in 2010 since our cruise tracks did not cover this part of the ridge (Figure 4).

There were no noticeable, short-term (hourly or daily) variations in flare activity from the pockmarks, indicating that gas venting was occurring continuously (Figure 4). Bubbles were detected to rise between 990 and 720 m above the seafloor to final water depths of 210 to 480 m, respectively (Figure 5). In 2010, the highest flare was observed at pockmark 2 and reached a height of 930 m and final water depth of only 270 mbsl. In 2012, the highest flare was detected at pockmark 6 and reached a height of 990 m (210 mbsl).

4.2. Gas Chimneys

At the seafloor, flares are connected to acoustically transparent zones in the sediment that extend from pockmarks to depths below the BSR (Figures 3a and 3b). These zones are up to 250 m wide and are slightly wider at their base than on top (Figure 3b). We interpret these conduits as "gas chimneys," or areas where free gas is migrating through the HSZ [*Bünz et al*., 2012]. Deep seismic reflection profiles suggest that these chimneys are fed by a critically pressured free-gas column beneath the BSR [*Bünz et al*., 2012; *Hustoft et al*., 2009]. High pore pressure at the crest of this gas column creates large enough forces to fracture the overlying material and pushes gas through the HSZ [*Cartwright et al*., 2007; *Flemings et al*., 2003]. Free-gas

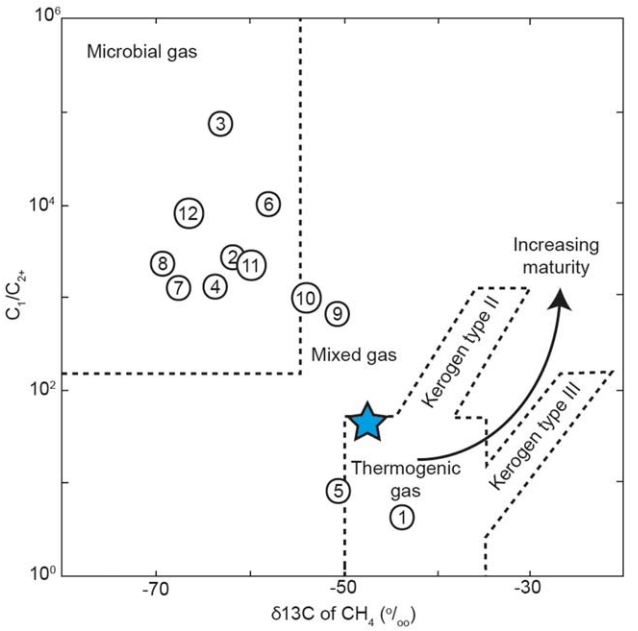

Figure 6. Hydrate-bound gas geochemistry from the Vestnesa Ridge and comparison to other high-flux regions. The fields of microbial, thermogenic, and mixed gases are defined after *Whiticar* [1999]. The gas geochemistry at the Vestnesa Ridge (blue star) suggests a mature thermogenic source. This geochemical signature is unique for high-flux regions. Point locations are from *Milkov* [2005]: (1) offshore Vancouver Island; (2) offshore Northern California; (3) offshore Sakhalin; (4) Black Sea; (5) Caspian Sea; (6) offshore Barbados; (7) offshore Georgia; (8) offshore Gabon; (9) Gulf of Mexico; (10) offshore Nigeria; (11) Norwegian Sea; and (12) offshore Oregon.

migration through these fractures may be maintained by lack of water to form hydrates, high salinities, and/or elevated temperatures [*Tréhu et al*., 2004]. Salinities and temperatures within gas chimneys can be elevated via the upward flow of warm, saline fluids from depth [*Ruppel et al*., 2005; *Wood et al*., 2002]. Alternatively, high salinities and temperatures can be generated via the exclusion of salt and release of latent heat during hydrate formation [*Liu and Flemings*, 2006, 2007].

Although the mechanism by which gas passes through the HSZ remains unclear, we are confident that these chimneys contain free gas as indicated by the presence of enhanced reflections and "push-down" features in the seismic data (Figure 3b). Furthermore, the fact that gas bubbles emanate from the seafloor where chimneys pierce the seafloor strongly suggests that the acoustic transparency in our seismic data is produced from the absorption and/or scattering of seismic energy from the presence of free gas. These vertical intrusions of free gas result in a rough BHSZ that extends from ~160 mbsf, where the BSR is clearly imaged, to just meters within the seafloor (Figure 3b). We map these lateral variations in the BHSZ such that the BHSZ encompasses features in the seismic data that we interpret to record free gas in the subseabed (e.g., enhanced reflections, "push-down" features, and acoustic transparency; Figure 3b). This approach is similar to that taken by *Wood et al*. [2002] at Hydrate Ridge, where gas intrusions into the HSZ result in a similar irregular BHSZ topography.

4.3. Gas Hydrate at Vestnesa

Piston coring (PC) and gravity coring (GC) recovered gas hydrate in 2–4 mbsf (GC929), carbonates (PC928), and Pogonophora tube worms (GC930; Figure 2). Gas hydrates had an average composition of methane (C_1, 96.31%), ethane (C_2, 3.36%), and small amounts of propane (C_3, 0.21%), isobutane (i-C_4, 0.11%), and n-butane (n-C_4, 0.01%). Both the C_1 and C_2 of the gas are isotopically enriched in ^{13}C with $\delta^{13}C$ values of $-47.7‰$ and $-26.35‰$, respectively. This is in agreement with the $-45.7‰$ value previously measured at one of the pockmarks in 2008 [*Fisher et al*., 2011].

4.3.1. Source of the Gas

The combination of the C_1/C_{2+} ratio (26.1), the $\delta^{13}C$ of C_1 and C_2 ($-47.7‰$ and $-26.35‰$), and the presence of C_{3+} gases suggests significant involvement of thermogenic processes [*Milkov*, 2005; *Whiticar*, 1999] (Figure 6). Specifically, gas is generated via thermal cracking of organic matter and/or oil at temperatures $>\sim150°C$, rather than by biogenic processes as is most commonly observed at high-flux sites (Figure 6) [*Milkov*, 2005]. The origin of this thermogenic gas in sediments above <20 Ma ocean crust remains unclear and is up to speculation. It may be produced from Early Miocene source rocks that derived from terrigenous organic-carbon rich deposits from the Svalbard hinterland that may be mature with respect to hydrocarbon generation on the Eastern basin margin [*Knies and Mann*, 2002]. The ridge's proximity to young and hot oceanic crust may be causing higher geothermal heat flow (via conduction), which is accelerating the maturation process. Alternatively, high heat flow via the flow of fluids (advection), associated with active

hydrothermal systems in the oceanic crust, may be penetrating marine sediments and maturing younger source rocks [*Judd and Hovland*, 2007].

An alternative interpretation is that gas and other fluids at the Vestnesa Ridge are sourced via serpentinization-driven migration of gas-rich fluids. This process has been invoked in a nearby free-gas and gas-hydrate system on the Knipovich Ridge to the South of our study area [*Rajan et al*., 2012]. Methane may be generated in ocean rift environments during the serpentinization of ultramafic rocks [*Cannat et al*., 2010; *Keir et al*., 2006, 2005; *Proskurowski et al*., 2008]. In the Arctic Ocean, exhumed ultramafic mantle rocks have been observed and sampled at the ultraslow Gakkel Ridge [*Dick et al*., 2003]. We, however, lack deeper seismic data allowing us to image gas-migration pathways between the gas-hydrate system at the Vestnesa Ridge and the oceanic crust, which is ~5 km below the seafloor. Furthermore, if the gas was sourced via serpentinization, we would expect our measured $\delta^{13}C$ values of CH_4 ($-47.7‰$) to be heavier and closer to average values for abiogenic methane ($\sim -25‰$) [*Judd and Hovland*, 2007]. *Keir et al*. [2005] report that methane in the water column can be as isotopically heavy as $-10‰$ and can be further changed due to biological oxidation to $+10‰$. We therefore consider the possibility of abiogenically produced methane unlikely at this northern location of the Vestnesa Ridge and favor the interpretation that gas at our study area is thermogenic. More detailed trace-gas analyses during upcoming sediment sampling will hopefully elucidate the different methane sources and their contribution to near-seafloor gas composition. Mixes of thermogenic, biogenic, and abiogenic methane are possible. Future hydrogen isotope analyses will further help to discriminate these different gas-producing mechanisms.

4.3.2. Estimating Composition of the Original Feed Gas From Gas Hydrates

Molecular fractionation occurs during gas-hydrate crystallization [*Sloan*, 1998], such that hydrates will be enriched in heavier hydrocarbons and depleted in C_1 compared to the original thermogenic feed gas that is supplied from below the HSZ. Structure I (SI) hydrates will preferentially incorporate C_2 over C_1, but will not incorporate heavier hydrocarbons ($>C_2$) due to their unfavorable molecular diameter [*Sloan*, 1998]. If sufficient quantities of heavier hydrocarbons exist in the feed gas, hydrates crystallize as structure II (SII) and incorporate larger gas molecules [*Sloan*, 1998]. The presence of trace amounts of C_3, n-C_4, and i-C_4 in our hydrate analyses indicates that some SII hydrates are crystallizing; however, the relatively low C_1/C_{2+} ratio of hydrates suggests that SI hydrates are also forming [*Sloan*, 1998].

We use the CSMYHD program [*Sloan*, 1998] to theoretically solve for the feed-gas composition necessary to form hydrates with the measured molecular gas composition. At seafloor pressure (~12.18 MPa), a feed-gas composition of 99% C_1, 0.84% C_2, and 0.16% C_3 will crystallize as SI hydrates with a composition of 96.75 C_1, 3.25% C_2, and 0% C_3. Whereas, a slightly different gas composition of 99% C_1, 0.82% C_2, and 0.18% C_3 will crystallize as SII hydrate with a substantially different composition: 91.03% C_1, 2.46% C_2, and 6.51% C_3 (Figure 7a). The measured gas composition of hydrates (96.31% C_1, 3.36% C_2, and 0.33% $>C_2$) is within the range of either SI or SII hydrates. We therefore assume that the thermogenic feed gas is within the range of the two feed compositions (Figure 7b). This feed gas is a first-order approximation since the gas composition varied slightly for the three samples measured. Regardless, minor changes in the feed-gas composition do not significantly affect the calculated depths of the BHSZ and THSZ. For example, a feed-gas composition of 99% C_1, 0.82% C_2, and 0.18% C_3 will result in the BHSZ being ~1 m deeper and the THSZ being ~7 m shallower than for a feed-gas composition of 99% C_1, 0.84% C_2, and 0.16% C_3.

4.4. Theoretical Hydrate Stability Zone

By constraining the composition of the feed gas, we can accurately model the HSZ based on sediment heat-flow measurements in the first few meters below the seafloor [*Sundvor et al*., 2000] and CTD water-column data (Figures 1 and 7b). We assume hydrostatic pressures and use the measured seawater salinity (3.5 wt%) at the seafloor during our CSMHYD calculations [*Sloan*, 1998] (Figure 7b). This approach predicts the BHSZ to be 155 m below seafloor (mbsf), which agrees well with the depth of the BSR (~162 mbsf if a 1.62 km s^{-1} acoustic velocity is assumed in the HSZ) [*Petersen et al*., 2010]. The slight (~8 m) mismatch between the predicted BHSZ and the BSR may be due to lateral variations in the geothermal gradient (i.e., the measured temperature gradient was not taken at the same location where we observe the BSR; Figures 1 and 3). Alternatively, the upward flow of fluids from depth may cause the measured subseafloor temperature gradient to decrease with depth [e.g., *Bredehoeft and Papaopulos*, 1965]. Such a concave-down temperature gradient would result in our predicted BHSZ being shallower than the observed BSR depth. The THSZ

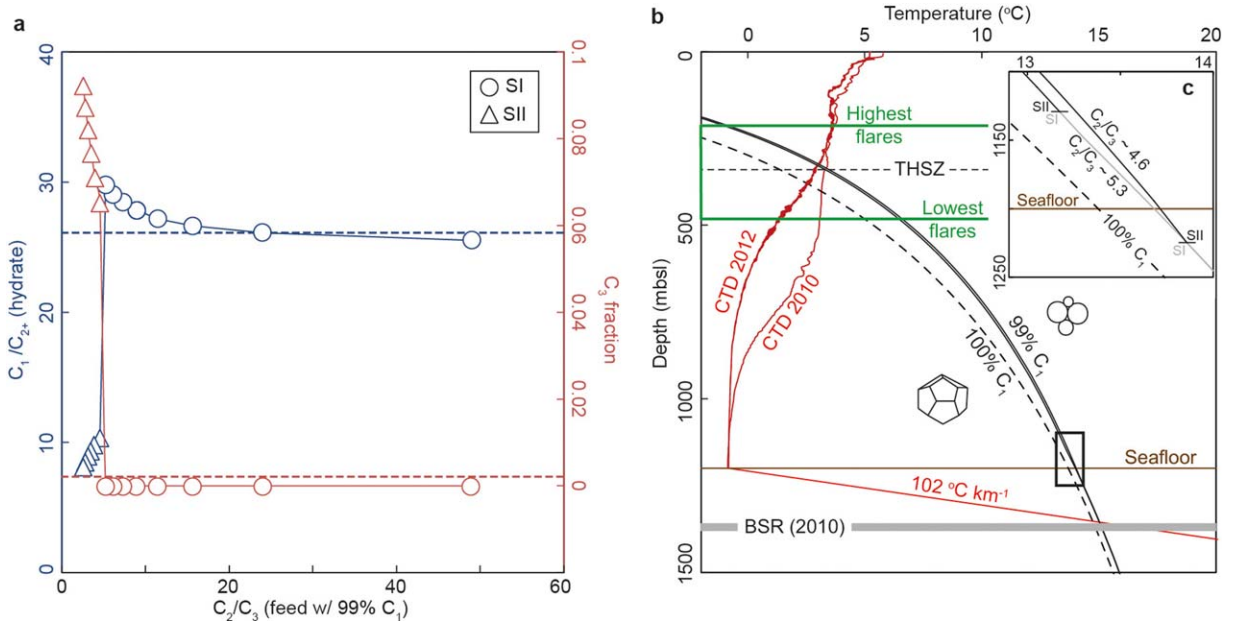

Figure 7. Calculation of the HSZ. (a) A feed-gas composition of 99% C_1, 0.96% C_2, and 0.04% C_3 will form hydrate with a C_1/C_{2+} ratio of 26.1, which is in agreement with the C_1/C_{2+} ratio measured in hydrates at the Vestnesa Ridge (26.1, dotted blue line). Hydrate forming from this gas mix, however, will not incorporate any C_3, which we measure in hydrates (0.21%, dotted red line). We add increasing amounts of C_3 to the feed-gas composition to determine the value at which hydrates will begin to incorporate the larger C_3 gas molecule. When the feed gas has a composition of 99% C_1, 0.82% C_2, 0.18% C_3, hydrate will begin to incorporate C_3. At this value, the gas no longer forms SI hydrates (circles), but forms SII hydrates (triangles). This change in lattice style causes 6.5% of the hydrate to be comprised of C_3, which is significantly higher than the measured mass percent (0.21%). We therefore propose that hydrates near the seafloor are some combination of SI and SII hydrates. (b) Hydrate stability curves for pure methane (dotted black line) and the feed-gas composition inferred from the gas composition measured in hydrate (solid black line). The temperature gradient in the first few meters below the seabed at the Vestnesa Ridge is 102°C km^{-1} [*Sundvor et al*., 2000]. The locations of the CTD profiles and the temperature-gradient measurement are shown in Figure 1. (c) At the seafloor, a feed composition of 99% C_1, 0.84% C_2, 0.16% C_3 will crystallize as SI hydrate (gray line), whereas a slightly different feed composition of 99% C_1, 0.82% C_2, 0.18% C_3 will form SII hydrate (black line).

is predicted to be 860 m above seafloor at only 340 m water depth (at a temperature of ~3.3°C), which shows good agreement with the analyzed flare heights (Figures 5a and 5b).

4.5. Hydrate Skins

The frequent observation of flare heights close to the calculated THSZ suggests that hydrate skins are developing around gas bubbles, decreasing gas-dissolution processes during bubble rise, and allowing bubbles to reach such heights [*Greinert et al*., 2006; *McGinnis et al*., 2006; *Rehder et al*., 2002, 2009]. Although estimates of bubble rising speeds could not be performed with available hydroacoustic data [e.g., *Artemov*, 2006; *Greinert et al*., 2006], we use the horizontal displacement of flares relative to the flares' rise height (here 0.4–0.5; Figure 3a) and a horizontal current speed of ~8 cm s^{-1} [*Fahrbach et al*., 2001] to estimate the vertical bubble rising speed to be between 16 and 20 cm s^{-1}. This rise speed is similar to that of hydrate-skinned bubbles with an 8.5–13 mm diameter detected in the Black Sea (19–22 cm s^{-1}) [*Greinert et al*., 2006]. Using the bubble-dissolution model of *McGinnis et al*. [2006] that considers hydrate-skin effects on bubble transport within the HSZ, we show that hydrate-skinned bubbles with a radius of 7–12 mm will reach the observed rise heights of 720 and 990 m, respectively (Figure 8). Such bubble sizes are reasonable and within the range observed near the seafloor at other locations (e.g., the Makran continental margin) [*Römer et al*., 2012].

Our bubble-modeling approach does not consider a possible upwelling flow, the influence of the low water temperature at the Vestnesa Ridge (−1°C), or the incorporation of C_2 and C_3 in the gas-hydrate skin. Thus, the estimated bubble-size range as well as rising speeds need to be seen as first-order approximations. So far, no bubbles have been visually recorded at the Vestnesa Ridge.

4.6. Variability of Gas Emissions

The processes driving seafloor gas expulsion at the Vestnesa Ridge remain elusive. In particular, we cannot determine if present-day gas emissions are sourced from below the HSZ, directly from hydrate dissociation, or some combination of the two processes. The recovery of methane-derived carbonates and a seep-

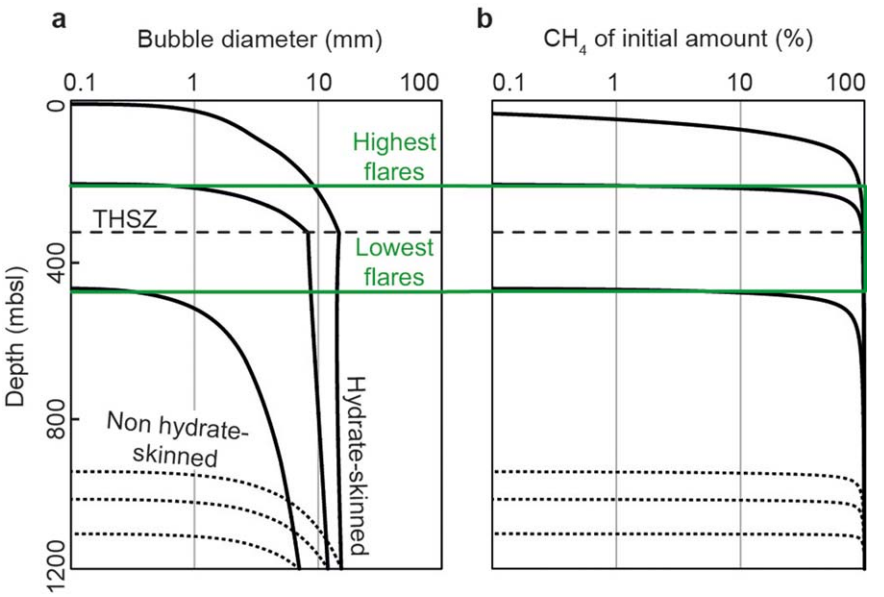

Figure 8. Model results for six different gas bubbles—three with hydrate skins (solid lines) and three without hydrate skins (dashed lines). (a) Initial bubbles sizes for the simulations are 7, 12, and 15.4 mm. Larger bubbles have a lower surface area to volume ratio, and therefore, their CH_4-transport efficiency is greater. The hydrate skin drastically decreases the mass-transfer coefficient, allowing bubbles to rise further and reach greater heights. To reach the detected flare height of 720–990 m, a methane hydrate-skinned bubble with an initial 7–12 mm diameter is necessary. (b) During the ascent of methane bubbles, methane is replaced by O_2 and N_2 dissolved in ocean water. All simulations were done using the SiBu-GUI program [*Greinert and McGinnis*, 2009], which allows GUI-based access to the model described by *McGinnis et al.* [2006].

specific biological community at the seafloor (Beggiatoa mats and Pogonopora fields; O. Pfannkuche, personal communication, 2011; RV Poseidon cruise POS419) implies a long-lived seep system (>1000 years) [*Luff and Wallmann*, 2003]. However, the presence of gas flares in 2010 and 2012, and their absence over the same area during cruises in 2006 and 2007 suggests that seafloor gas expulsion may have increased recently [*Bünz et al.*, 2012; *Hustoft et al.*, 2009]. This could be due to natural variability in the subsurface plumbing and subsequent gas migration of the critically pressured free-gas reservoir [*Bangs et al.*, 2011]. Alternatively, the increase may be due to the dissociation of gas hydrate caused by intermittent hydrothermal pulses from the underlying <20 Ma oceanic crust [*Hustoft et al.*, 2009] or decadal-scale ocean warming that has occurred recently in the region [*Ferré et al.*, 2012].

5. Inferred Implications

5.1. Methane Delivery to the Upper Ocean and Atmosphere

Other deepwater high-flux seep sites expel mostly biogenic gas into relatively warm water masses, resulting in a THSZ at greater water depth (>450 mbsl; Figures 6 and 9). At these sites, hydrate-skinned bubbles reach water depths of 350–1850 mbsl (Figure 9). In contrast, the Vestnesa Ridge expels thermogenic gas into cool water masses, resulting in a shallow THSZ (at 340 mbsl). Consequently, hydrate-skinned thermogenic gas bubbles rise to shallower water depths than observed previously (Figure 9). This result suggests that a previously unacknowledged supply of methane carbon may be transferred to the upper ocean from the Arctic deepwater (Figure 10). Some deepwater vents in the Gulf of Mexico may release bubbles all the way to the atmosphere [*Solomon et al.*, 2009], but bubble transport at these locations is further aided by oil as surfactant that additionally reduces dissolution processes at water depths shallower than the THSZ [*Leifer and Macdonald*, 2003].

Methane released into the upper ocean may be a significant factor in controlling ocean chemistry. During ascent, methane bubbles, with or without hydrate skins, dissolve methane and strip N_2 and O_2 from the water. As a result only a small fraction of the methane released at the seafloor reaches the maximum height of observed flares (Figure 8b) [*Leifer and Patro*, 2002]. However, the model suggests that some of the methane released at the seafloor is transported to the upper ocean mixed layer which is >400 m offshore

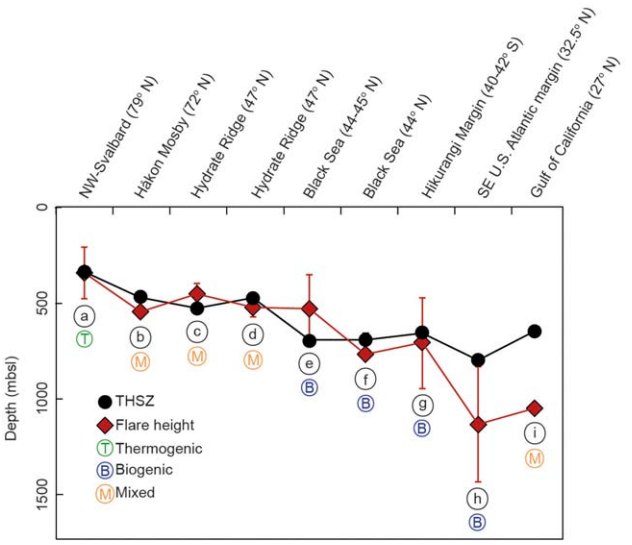

Figure 9. Comparison of flare heights and the THSZ at the Vestnesa Ridge to other deepwater venting locations. Colder water masses and thermogenic gas offshore high-latitude W-Svalbard create a THSZ that is significantly shallower than that observed at other deepwater locations. As a result, gas flares offshore W-Svalbard extend to depths shallower than have been observed previously. Data are from: (a) this study; (b) [*Lein et al.*, 1999; *Sauter et al.*, 2006]; (c) [*Kannberg et al.*, 2013; *Milkov et al.*, 2005]; (d) [*Heeschen et al.*, 2003; *Milkov et al.*, 2005]; (e) [*Milkov*, 2005; *Römer et al.*, 2012]; (f) [*Greinert et al.*, 2006; *Milkov*, 2005]; (g) [*Faure et al.*, 2010; *Greinert et al.*, 2010]; (h) [*Brothers et al.*, 2013; *Paull et al.*, 1995]; (i) [*Merewether et al.*, 1985; *Simoneit et al.*, 1982].

NW-Svalbard [*de Boyer Montégut et al.*, 2004], and bubbles with initially large diameters (>15 mm) will transport methane directly to the atmosphere (Figure 8b). Methane that dissolves in the water column may be oxidized microbially [*Kessler et al.*, 2011; *Valentine et al.*, 2001], which lowers the ocean-water pH value (i.e., makes it less alkaline) and can lead to the ultimate release of CO_2 to the atmosphere [*Biastoch et al.*, 2011; *Ruppel*, 2011]. Conversely, methane that reaches the winter mixed layer might be transported to the atmosphere on time scales shorter than the microbial turnover time in the ocean [*Solomon et al.*, 2009]. The injection of methane carbon to the upper ocean also has a beneficiary effect. Elevated CO_2 can fuel photosynthesizing biological communities in the near-surface water, and this benefit can then propagate down the food chain from primary to secondary producers [*Hovland*, 2012; *Hovland et al.*, 2012].

5.2. Hydrate Reservoir Stability

A common view of deepwater hydrate systems is that free gas, water, and hydrate theoretically coexist at two depths: the THSZ and the BHSZ. In this stratified system, a temperature increase imposed at the seafloor will take 100–1000 years to thermally equilibrate within the HSZ [*Reagan and Moridis*, 2007; *Ruppel*, 2011]. Additionally, once thermal equilibration occurs, gas released from hydrate dissociation at the BHSZ might be trapped in newly formed gas hydrate or microbially consumed in the sulfate reduction zone [*Boetius et al.*, 2000; *Reagan and Moridis*, 2007]. In contrast to this stratified system, free gas migrates through vertical conduits to the seafloor, and as a result the BHSZ exhibits significant topography (Figures 3b and 10). The implications of this rough hydrate-phase boundary are twofold. First, since in some chimneys the BHSZ appears to extend within <10 m below the seafloor (which is approximately the vertical resolution of our P-Cable data), a seafloor temperature increase will destabilize hydrates on time scales of just years, yielding a rapid methane flux to the ocean [*Reagan and Moridis*, 2007]. For example, using simple dimensional analysis and assuming a thermal diffusivity of 10^{-6} m^2 s^{-1} [*Rempel and Buffett*, 1997], we estimate that a temperature change at the seafloor will equilibrate over a 10 m distance in the sediment column in ~3 years. Second, much of the methane released from dissociating hydrates will bypass the HSZ through free-gas conduits without forming new hydrate.

Although the vertical intrusions of gas into the HSZ suggest the deepwater hydrate reservoir may be more sensitive to ocean warming than previously thought, the hazard of hydrate-associated methane expulsion remains questionable. A seafloor-warming event at the Vestnesa Ridge would result in a dissociation scenario in which the already shoaled BHSZ is raised further toward the seafloor. This warming scenario means that the thinnest and therefore fastest-dissociating regions would be those containing the least hydrate (since the BHSZ is closest to the seafloor). Thus, the most sensitive hydrates would also be the least productive in terms of gas generation. Furthermore, the gas-rich intrusions that we outline in Figure 3b are nearly vertical, placing the bulk of the hydrate reservoir further from the seafloor and from the source of temperature change. It is therefore possible that the potential methane-release hazard at the Vestnesa Ridge may

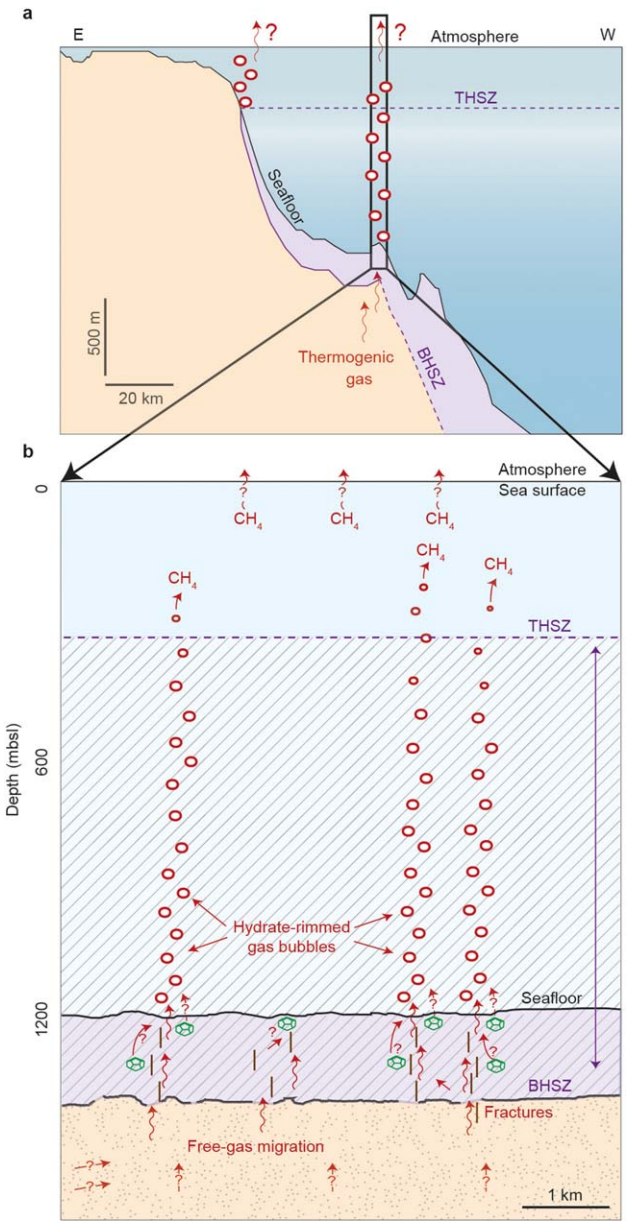

Figure 10. Conceptual view of the venting system at the Vestnesa Ridge. (a) cross section highlights (black box) location of the Vestnesa Ridge on the continental margin offshore W-Svalbard. (b) Thermogenic free gas (red arrows) is sourced from beneath the BSR and migrates to the crest of the BSR anticline (Figure 1) [*Hustoft et al.*, 2009; *Vogt et al.*, 1994]. There it accumulates until gas pressure becomes high enough to dilate fractures, prompting vertical gas migration through the HSZ [*Flemings et al.*, 2003; *Hornbach et al.*, 2004; *Hubbert and Willis*, 1972]. Some gas may also be sourced directly from the melting of hydrates (green cages) within the HSZ due to decadal-scale ocean warming [*Westbrook et al.*, 2009] and/or pulses of hydrothermal activity from underlying, young oceanic crust [*Bünz et al.*, 2012; *Hustoft et al.*, 2009]. Hydrate-skinned gas bubbles are released from pockmarks at the seafloor. The hydrate skin reduces dissolution processes, allowing bubbles to reach heights greater than the THSZ. This thermogenic gas seepage represents a new source of methane injection into the upper ocean and possibly atmosphere in the Arctic.

be due more to the uncapping of an underlying thermogenic methane source with a gas chimney acting as a gas-migration conduit.

6. Summary

We present new gas-hydrate geochemistry analyses from the gas-hydrate charged Vestnesa Ridge in the Fram Strait, the only deepwater gateway to the Arctic Ocean. We show that a thermogenic source is supplying methane and other light hydrocarbons to the Vestnesa Ridge. New echosounder data reveal that at least 4, and up to 6 pockmarks, were continuously releasing hydrate-rimmed gas bubbles during 4–5 day cruises in 2010 and 2012. The thermogenic gas composition together with cool water masses (~3.3°C) at the Vestnesa Ridge create an abnormally shallow THSZ, allowing the hydrate-rimmed gas bubbles released from the seabed at ~1200 m water depth to reach shallow water depths within the ocean mixing zone. Our revised interpretation of three-dimensional P-Cable seismic data at the Vestnesa Ridge suggests that acoustically transparent zones within the HSZ record free-gas migration through the HSZ and cause significant lateral variations in the BHSZ. Such irregular topography of the BHSZ may result in enhanced sensitivity of the Vestnesa Ridge to Arctic Ocean warming.

7. Future Work

The Centre of Excellence for Arctic Gas Hydrate, Environment and Climate (CAGE) at UiT The Arctic University of Norway will be dedicated to understanding the effect that Arctic gas hydrates have on the environment and climate in the northern hemisphere. CAGE was opened in November 2013 by the Research Council of Norway and will receive 10 years of funding to perform long-term monitoring of Arctic gas-hydrate charged regions included the Vestnesa Ridge. Future data collection will ultimately constrain

(1) the short and long-term variability of gas release, (2) the sensitivity of the hydrate reservoir to warming at the seafloor, and (3) the impact of both shallow and deepwater methane release on oceanic and atmospheric budgets and marine ecosystems.

Acknowledgments
The research is part of the Centre of Excellence: Arctic Gas Hydrate, Environment and Climate (CAGE) funded by the Norwegian Research Council (grant 223259). A. Smith was supported by a Fulbright fellowship through the U.S.-Norway Fulbright Foundation. We thank D. McGinnis for discussions regarding the bubble-dissolution model, as well as M. Schmidt from GEOMAR and M. Krüger from BGR for doing isotope analyses. We also thank M. Hovland, A. Portnov, and an anonymous reviewer for detailed and constructive comments that greatly improved the manuscript.

References

Artemov, Y. (2006), Software support for investigation of natural methane seeps by hydroacoustic method, *Mar. Ecol. J.*, *5*, 57–71.
Bangs, N. L. B., M. J. Hornbach, and C. Berndt (2011), The mechanics of intermittent methane venting at South Hydrate Ridge inferred from 4D seismic surveying, *Earth Planet. Sci. Lett.*, *310*(1–2), 105–112.
Berndt, C., et al. (2014), Temporal constraints on hydrate-controlled methane seepage off Svalbard, *Science*, *343*(6168), 284–287.
Biastoch, A., et al. (2011), Rising Arctic Ocean temperatures cause gas hydrate destabilization and ocean acidification, *Geophys. Res. Lett.*, *38*, L08602, doi:10.1029/2011GL047222.
Boetius, A., K. Ravenschlag, C. J. Schubert, D. Rickert, F. Widdel, A. Gieskes, R. Amann, B. B. Joergensen, U. Witte, and O. Pfannkuche (2000), A microbial consortium apparently mediating anaerobic oxidation of methane, *Nature*, *407*, 623–626.
Bredehoeft, J. D., and I. S. Papaopulos (1965), Rates of vertical groundwater movement estimated from the Earth's thermal profile, *Water Resour. Res.*, *1*(2), 325–328.
Brothers, L. L., C. L. Van Dover, C. R. German, C. L. Kaiser, D. R. Yoerger, C. D. Ruppel, E. Lobecker, A. D. Skarke, and J. K. S. Wagner (2013), Evidence for extensive methane venting on the southeastern U.S. Atlantic margin, *Geology*, *41*, 807–810.
Bünz, S., S. Polyanov, S. Vadakkepuliyambatta, C. Consolaro, and J. Mienert (2012), Active gas venting through hydrate-bearing sediments on the Vestnesa Ridge, offshore W-Svalbard, *Mar. Geol.*, *332–334*, 189–197.
Cannat, M., F. Fontaine, and J. Escartin (2010), Serpentinization and associated hydrogen methane fluxes at slow spreading ridges, *Geophys. Monogr. Ser.*, *188*, 241–264.
Cartwright, J., M. Huuse, and A. Aplin (2007), Seal bypass systems, *AAPG Bull.*, *91*, 1141–1166.
Damm, E., A. Mackensen, G. Budéus, E. Faber, and C. Hanfland (2005), Pathways of methane in seawater: Plume spreading in an Arctic shelf environment (SW-Spitsbergen), *Cont. Shelf Res.*, *25*(12–13), 1453–1472.
de Boyer Montégut, C., G. Madec, A. S. Fischer, A. Lazar, and D. Iudicone (2004), Mixed layer depth over the global ocean: An examination of profile data and a profile-based climatology, *J. Geophys. Res.*, *109*, C12003, doi:10.1029/2004JC002378.
Dick, J. B. H., J. Lin, and H. Schouten (2003), An ultraslow-spreading class of ocean ridge, *Nature*, *426*, 405–412.
Dickens, G. R. (2003), Rethinking the global carbon cycle with a large, dynamic and microbially mediated gas hydrate capacitor, *Earth Planet. Sci. Lett.*, *213*(3–4), 169–183.
Eiken, O., and K. Hinz (1993), Contourites in the Fram Strait, *Sediment. Geol.*, *82*(1-4), 8215–8232.
Fahrbach, E., J. Meincke, S. Østerhus, G. Rohardt, U. Schauer, V. Tverberg, and J. Verduin (2001), Direct measurements of volume transports through Fram Strait, *Polar Res.*, *20*(2), 217–224.
Faure, K., J. Greinert, J. Schneider von Deimling, D. F. McGinnis, R. Kipfer, and P. Linke (2010), Methane seepage along the Hikurangi Margin of New Zealand: Geochemical and physical data from the water column, sea surface and atmosphere, *Mar. Geol.*, *272*(1–4), 170–188.
Ferré, B., J. Mienert, and T. Feseker (2012), Ocean temperature variability for the past 60 years on the Norwegian-Svalbard margin influences gas hydrate stability on human time scales, *J. Geophys. Res.*, *117*, C10017, doi:10.1029/2012JC008300.
Fisher, R. E., et al. (2011), Arctic methane sources: Isotopic evidence for atmospheric inputs, *Geophys. Res. Lett.*, *38*, L21803, doi:10.1029/2011GL049319.
Flemings, P. B., X. Liu, and W. J. Winters (2003), Critical pressure and multiphase flow in Blake Ridge gas hydrates, *Geology*, *31*(12), 1057–1060.
Gentz, T., E. Damm, J. Schneider von Deimling, S. Mau, D. F. McGinnis, and M. Schlüter (2014), A water column study of methane around gas flares located at the West Spitsbergen continental margin, *Cont. Shelf Res.*, *72*, 107–118.
Graversen, R. G., T. Mauritsen, M. Tjernstrom, E. Kallen, and G. Svensson (2008), Vertical structure of recent Arctic warming, *Nature*, *451*(7174), 53–56.
Greinert, J., and D. F. McGinnis (2009), Single bubble dissolution model – The graphical user interface SiBu-GUI, *Environ. Modell. Software*, *24*(8), 1012–1013.
Greinert, J., Y. Artemov, V. N. Egorov, M. De Batist, and D. F. McGinnis (2006), 1300-m-high rising bubbles from mud volcanoes at 2080 m in the Black Sea: Hydroacoustic characteristics and temporal variability, *Earth Planet. Sci. Lett.*, *244*(1–2), 1–15.
Greinert, J., K. B. Lewis, J. Bialas, I. A. Pecher, A. Rowden, D. A. Bowden, M. De Batist, and P. Linke (2010), Methane seepage along the Hikurangi Margin, New Zealand: Overview of studies in 2006 and 2007 and new evidence from visual, bathymetric and hydroacoustic investigations, *Mar. Geol.*, *272*(1–4), 6–25.
Heeschen, K. U., A. M. Tréhu, R. W. Collier, E. Suess, and G. Rehder (2003), Distribution and height of methane bubble plumes on the Cascadia Margin characterized by acoustic imaging, *Geophys. Res. Lett.*, *30*(12), 1643, doi:10.1029/2003GL016974.
Hornbach, M. J., D. M. Saffer, and W. Steven Holbrook (2004), Critically pressured free-gas reservoirs below gas-hydrate provinces, *Nature*, *427*(6970), 142–144.
Hovland, M. (2012), Marine life associated with offshore drilling, pipelines, and platforms, in *Encyclopedia of Sustainability Science and Technology*, edited by R.A. Meyers, p. 30, Springer, New York.
Hovland, M., J. Jensen, and C. Fichler (2012), Methane and minor oil macro-seep systems: Their complexity and environmental significance, *Mar. Geol.*, *332–334*, 163–173.
Hubbert, M. K., and D. G. Willis (1972), Mechanics of hydraulic fracturing, *Mem. Am. Assoc. Pet. Geol.*, *18*, 239–257.
Hustoft, S., S. Bünz, J. Mienert, and S. Chand (2009), Gas hydrate reservoir and active methane-venting province in sediments on <20 Ma young oceanic crust in the Fram Strait, offshore NW-Svalbard, *Earth Planet. Sci. Lett.*, *284*(1–2), 12–24.
Judd, A. G., and M. Hovland (2007), *Seabed Fluid Flow: The Impact on Geology, Biology, and the Marine Environment*, 475 pp., Cambridge Univ. Press, Cambridge.
Kannberg, P. K., A. M. Tréhu, S. D. Pierce, C. K. Paull, and D. W. Caress (2013), Temporal variation of methane flares in the ocean above Hydrate Ridge, Oregon, *Earth Planet. Sci. Lett.*, *368*, 33–42.
Kayen, R. E., and H. J. Lee (1991), Pleistocene slope instability of gas hydrate-laden sediment on the Beaufort sea margin, *Mar. Geotechnol.*, *10*(1–2), 125–141.
Keir, R. S., J. Greinert, M. Rhein, G. Petrik, J. Sültenfuß, and K. Fürhaupter (2005), Methane and methane carbon isotope ratios in the northeast Atlantic including the Mid-Atlantic Ridge (50°N), *Deep Sea Res., Part I*, *52*, 1043–1070.

Keir, R. S., J. Sültenfuß, M. Rhein, G. Petrik, and J. Greinert (2006), Separation of 3He and CH4 signals on the Mid-Atlantic Ridge at 5°N and 51°N, *Geochim. Cosmochim. Acta*, *70*(23), 5766–5778.
Kennett, J. P., K. G. Cannariato, I. L. Hendy, and R. J. Behl (2000), Carbon isotopic evidence for methane hydrate instability during quaternary interstadials, *Science*, *288*(5463), 128–133.
Kessler, J. D., et al. (2011), A persistent oxygen anomaly reveals the fate of spilled methane in the deep Gulf of Mexico, *Science*, *331*(6015), 312–315.
Knies, J., and U. Mann (2002), Depositional environment and source rock potential of Miocene strata from the central Fram Strait: Introduction of a new computing tool for simulating organic facies variations, *Mar. Pet. Geol.*, *19*(7), 811–828.
Leifer, I., and I. R. Macdonald (2003), Dynamics of the gas flux from shallow gas hydrate deposits: Interaction between oily hydrate bubbles and the oceanic environment, *Earth Planet. Sci. Lett.*, *210*(3–4), 411–424.
Leifer, I., and R. K. Patro (2002), The bubble mechanism for methane transport from the shallow sea bed to the surface: A review and sensitivity study, *Cont. Shelf Res.*, *22*(16), 2409–2428.
Lein, A., P. Vogt, K. Crane, A. Egorov, and M. Ivanov (1999), Chemical and isotopic evidence for the nature of the fluid in CH4-containing sediments of the Håkon Mosby Mud Volcano, *Geo-Mar. Lett.*, *19*(1–2), 76–83.
Liu, X., and P. B. Flemings (2006), Passing gas through the hydrate stability zone at southern Hydrate Ridge, offshore Oregon, *Earth Planet. Sci. Lett.*, *241*(1–2), 211–226.
Liu, X., and P. B. Flemings (2007), Dynamic multiphase flow model of hydrate formation in marine sediments, *J. Geophys. Res.*, *112*, B03101, doi:10.1029/2005JB004227.
Lonsdale, P., and K. Becker (1985), Hydrothermal plumes, hot springs, and conductive heat flow in the Southern Trough of Guaymas Basin, *Earth Planet. Sci. Lett.*, *73*(2–4), 211–225.
Luff, R., and K. Wallmann (2003), Fluid flow, methane fluxes, carbonate precipitation and biogeochemical turnover in gas hydrate-bearing sediments at Hydrate Ridge, Cascadia Margin: Numerical modeling and mass balances, *Geochim. Cosmochim. Acta*, *67*(18), 3403–3421.
Marín-Moreno, H., T. A. Minshull, G. K. Westbrook, B. Sinha, and S. Sarkar (2013), The response of methane hydrate beneath the seabed offshore Svalbard to ocean warming during the next three centuries, *Geophys. Res. Lett.*, *40*, 5159–5163, doi:10.1002/grl.50985.
McGinnis, D. F., J. Greinert, Y. Artemov, S. E. Beaubien, and A. Wüest (2006), Fate of rising methane bubbles in stratified waters: How much methane reaches the atmosphere?, *J. Geophys. Res.*, *111*, C09007, doi:10.1029/2005JC003183.
Merewether, R., M. S. Olsson, and P. Lonsdale (1985), Acoustically detected hydrocarbon plumes rising from 2-km depths in Guaymas Basin, Gulf of California, *J. Geophys. Res.*, *90*(B4), 3075–3085.
Mienert, J., M. Vanneste, S. Bünz, K. Andreassen, H. Haflidason, and H. P. Sejrup (2005), Ocean warming and gas hydrate stability on the mid-Norwegian margin at the Storegga slide, *Mar. Pet. Geol.*, *22*(1–2), 233–244.
Milkov, A. V. (2005), Molecular and stable isotope compositions of natural gas hydrates: A revised global dataset and basic interpretations in the context of geological settings, *Org. Geochem.*, *36*(5), 681–702.
Milkov, A. V., and R. Sassen (2002), Economic geology of offshore gas hydrate accumulations and provinces, *Mar. Pet. Geol.*, *19*(1), 1–11.
Milkov, A. V., G. E. Claypool, Y. J. Lee, and R. Sassen (2005), Gas hydrate systems at Hydrate Ridge offshore Oregon inferred from molecular and isotopic properties of hydrate-bound and void gases, *Geochim. Cosmochim. Acta*, *69*(4), 1007–1026.
Paull, C. K., W. Ussler, W. S. Borowski, and F. N. Spiess (1995), Methane-rich plumes on the Carolina continental rise: Associations with gas hydrates, *Geology*, *23*(1), 89–92.
Petersen, C. J., S. Bünz, S. Hustoft, J. Mienert, and D. Klaeschen (2010), High-resolution P-Cable 3D seismic imaging of gas chimney structures in gas hydrated sediments of an Arctic sediment drift, *Mar. Pet. Geol.*, *27*(9), 1981–1994.
Phrampus, B. J., and M. J. Hornbach (2012), Recent changes to the Gulf Stream causing widespread gas hydrate destabilization, *Nature*, *490*(7421), 527–530.
Proskurowski, G., M. D. Lilley, J. S. Seewald, G. L. Früh-Green, E. J. Olson, J. E. Lupton, S. P. Sylva, and D. S. Kelly (2008), Abiogenic hydrocarbon production at lost city hydrothermal field, *Science*, *319*, 604–607.
Rajan, A., J. Mienert, S. Bünz, and S. Chand (2012), Potential serpentinization, degassing, and gas hydrate formation at a young (<20 Ma) sedimented ocean crust of the Arctic Ocean ridge system, *J. Geophys. Res.*, *117*, B03102, doi:10.1029/2011JB008537.
Reagan, M. T., and G. J. Moridis (2007), Oceanic gas hydrate instability and dissociation under climate change scenarios, *Geophys. Res. Lett.*, *34*, L22709, doi:10.1029/2007GL031671.
Reeburgh, W. S. (2007), Oceanic methane biogeochemistry, *Chem. Rev.*, *107*, 486–513.
Rehder, G., P. W. Brewer, E. T. Peltzer, and G. Friederich (2002), Enhanced lifetime of methane bubble streams within the deep ocean, *Geophys. Res. Lett.*, *29*(15), 21–21–21–24.
Rehder, G., I. Leifer, P. G. Brewer, G. Friederich, and E. T. Peltzer (2009), Controls on methane bubble dissolution inside and outside the hydrate stability field from open ocean field experiments and numerical modeling, *Mar. Chem.*, *114*(1), 19–30.
Rempel, A. W., and B. A. Buffett (1997), Formation and accumulation of gas hydrate in porous media, *J. Geophys. Res.*, *102*(B5), 10,151–10,164.
Römer, M., H. Sahling, T. Pape, A. Bahr, T. Feseker, P. Wintersteller, and G. Bohrmann (2012), Geological control and magnitude of methane ebullition from a high-flux seep area in the Black Sea: The Kerch seep area, *Mar. Geol.*, *319–322*, 57–74.
Ruppel, C. (2011), Methane hydrates and contemporary climate change, *Nat. Educ. Knowl.*, *3*(10), 29.
Ruppel, C., G. R. Dickens, D. G. Castellini, W. Gilhooly, and D. Lizarralde (2005), Heat and salt inhibition of gas hydrate formation in the northern Gulf of Mexico, *Geophys. Res. Lett.*, *32*, L04605, doi:10.1029/2004GL021909.
Sauter, E. J., S. I. Muyakshin, J.-L. Charlou, M. Schlüter, A. Boetius, K. Jerosch, E. Damm, J.-P. Foucher, and M. Klages (2006), Methane discharge from a deep-sea submarine mud volcano into the upper water column by gas hydrate-coated methane bubbles, *Earth Planet. Sci. Lett.*, *243*(3–4), 354–365.
Schiermeier, Q. (2008), Fears surface over methane leaks, in *Nature News*, pp. 572–573, Nature News, London, UK.
Shakhova, N., et al. (2013), Ebullition and storm-induced methane release from the East Siberian Arctic Shelf, *Nat. Geosci.*, *7*, 64–70.
Simoneit, B. R. T., C. P. Summerhayesa, and P. A. Meyers (1982), Sources, preservation, and maturation of organic matter in Pliocene and Quaternary sediments of the Gulf of California: A synthesis of organic geochemical studies from deep sea drilling project leg 64, report #40, pp. 939–951, Ocean Drill. Program, College Station, TX.
Sloan, E. D. (1998), *Clathrate Hydrates of Natural Gases*, 2nd ed., 705 pp., Marcel Dekker, New York.
Solomon, E. A., M. Kastner, I. R. MacDonald, and I. Leifer (2009), Considerable methane fluxes to the atmosphere from hydrocarbon seeps in the Gulf of Mexico, *Nat. Geosci.*, *2*(8), 561–565.
Sundvor, E., O. Eldholm, T. Gladczenko, and S. Planke (2000), Norwegian-Greenland Sea thermal field, in *Dynamics of the Norwegian Margin*, edited by A. Nøttvedt et al., *Geol. Soc. Spec. Publ.*, 167, pp. 397–410.

Tréhu, A. M., P. B. Flemings, N. L. Bangs, J. Chevallier, E. Gràcia, J. E. Johnson, C. S. Liu, X. Liu, M. Riedel, and M. E. Torres (2004), Feeding methane vents and gas hydrate deposits at south Hydrate Ridge, *Geophys. Res. Lett.*, *31*, L23310, doi:10.1029/2004GL021286.

Valentine, D. L., D. C. Blanton, W. S. Reeburgh, and M. Kastner (2001), Water column methane oxidation adjacent to an area of active hydrate dissociation, Eel river Basin, *Geochim. Cosmochim. Acta*, *65*(16), 2633–2640.

Vogt, P. R., K. Crane, E. Sundvor, M. D. Max, and S. L. Pfirman (1994), Methane-generated(?) pockmarks on young, thickly sedimented oceanic crust in the Arctic: Vestnesa ridge, *Fram strait, Geology*, *22*(3), 255–258.

Westbrook, G. K., et al. (2009), Escape of methane gas from the seabed along the West Spitsbergen continental margin, *Geophys. Res. Lett.*, *36*, L15608, doi:10.1029/2009GL039191.

Whiticar, M. J. (1999), Carbon and hydrogen isotope systematics of bacterial formation and oxidation of methane, *Chem. Geol.*, *161*(1–3), 291–314.

Wood, W. T., J. F. Gettrust, N. R. Chapman, G. D. Spence, and R. D. Hyndman (2002), Decreased stability of methane hydrates in marine sediments owing to phase-boundary roughness, *Nature*, *420*(6916), 656–660.